Inorg. Chem. **2007**, *46*, 10594–10606

Unraveling the Reactive Species of a Functional Non-Heme Iron Monooxygenase Model Using Stopped-Flow UV–Vis Spectroscopy

Gerard T. Rowe,[†] Elena V. Rybak-Akimova,[‡] and John P. Caradonna*[,†]

Department of Chemistry, Boston University, Boston, Massachusetts 02215, Department of Chemistry, Tufts University, Medford, Massachusetts 02115

Received June 7, 2007

Low-temperature stopped-flow electronic spectroscopy was utilized to resolve the intermediates formed in the reaction of a diiron(II) compound, $Fe_2(H_2Hbamb)_2(N\text{-MeIm})_2$ (H_4HBamb = 2,3-bis(2-hydroxybenzamido)dimethylbutane), **1**, with the oxygen atom donors 2,6-dimethyliodosylbenzene and *p*-cyanodimethylaniline *N*-oxide and the mechanistic probe hydroperoxide 2-methyl-1-phenylprop-2-yl hydroperoxide (MPPH). Previous studies showed that **1** is capable of catalytically oxidizing cyclohexane to cyclohexanol (300 turnovers) via a pathway involving the heterolytic cleavage of the O–O bond of MPPH (>98% peroxide utilization). We now report intimate details of the formation of the reactive intermediate and its subsequent decay in the absence of substrates. The reaction, which is independent of the nature of the oxidant, proceeds in three consecutive steps assigned as (i) oxygen-atom transfer to one of the iron centers of **1** to form an Fe^{IV}═O species, **2**, (ii) ligand rearrangement to **3**, and (iii) internal collapse of the terminal oxo group to generate a diferric, μ-oxo species, **4**. Assignment of the second step as a ligand rearrangement was corroborated by stopped-flow spectroscopic studies of the one-electron oxidation of the starting diferrous **1**, which is also known to undergo ligand rearrangement upon the formation of the [Fe^{II}, Fe^{III}] mixed-valent complex. Observation of the reaction rates over a temperature range allowed for the determination of activation parameters for each of the three steps. The role of the ligand reorganization in the energetic profile for the formation of the catalytically competent intermediate is discussed, along with the potential biological significance of the internal conversion of the active oxidant to the inert, μ-oxo diiron(III) dimer, **4**.

Introduction

Significant interest in modeling[1−3] the reactivity properties of the class I family of diiron monooxygenases[4−6] (e.g., soluble methane monooxygenase, sMMO; R2 subunit of type 2 ribonucleotide reductase; Δ^9-desaturase) developed following the recognition of the unusual nature of the chemical transformations performed by these enzymes and the subsequent spectroscopic and structural characterizations of their binuclear, non-heme iron active sites. The monooxygenase members of this family are proposed to utilize a common high-valent iron−oxygen atom species ([Fe^{III},Fe^{V}═O] ⟷ [Fe^{IV},Fe^{IV}═O], [$Fe^{IV}(\mu\text{-O})_2Fe^{IV}$]) to oxidize substrates with high bond strengths, such as methane, the aryl C−H bonds of toluene, and saturated fatty acids.[5,7−9]

Detailed stopped-flow kinetic studies of the catalytic cycle of sMMO suggest that the reaction of dioxygen with the diferrous form of the enzyme generates a diferric peroxo species, **P**, that converts to the catalytically competent reactive intermediate, **Q** (kinetic **Q**).[10−13] Subsequent Möss-

* To whom correspondence should be addressed. E-mail: caradonn@bu.edu.
[†] Boston University.
[‡] Tufts University.

(1) Fontecave, M.; Menage, S.; Duboc-Toia, C. *Coord. Chem. Rev.* **1998**, *180*, 1555−1572.
(2) Tshuva, E. Y.; Lippard, S. J. *Chem. Rev.* **2004**, *104*, 987−1011.
(3) Costas, M.; Mehn, M. P.; Jensen, M. P.; Que, L. *Chem. Rev.* **2004**, *104*, 939−986.
(4) Colby, J.; Dalton, H. *Biochem. J.* **1976**, *157*, 495−497.
(5) Wallar, B. J.; Lipscomb, J. D. *Chem. Rev.* **1996**, *96*, 2625−2657.
(6) Ericson, A.; Hedman, B.; Hodgson, K. O.; Green, J.; Dalton, H.; Bentsen, J. G.; Beer, R. H.; Lippard, S. J. *J. Am. Chem. Soc.* **1988**, *110*, 2330−2332.
(7) Shu, L. J.; Nesheim, J. C.; Kauffmann, K.; Munck, E.; Lipscomb, J. D.; Que, L. *Science* **1997**, *275*, 515−518.
(8) Kopp, D. A.; Lippard, S. J. *Curr. Opin. Chem. Biol.* **2002**, *6*, 568−576.
(9) Riggs-Gelasco, P. J.; Shu, L. J.; Chen, S. X.; Burdi, D.; Huynh, B. H.; Que, L.; Stubbe, J. *J. Am. Chem. Soc.* **1998**, *120*, 849−860.
(10) Lee, S. K.; Fox, B. G.; Froland, W. A.; Lipscomb, J. D.; Munck, E. *J. Am. Chem. Soc.* **1993**, *115*, 6450−6451.
(11) Priestley, N. D.; Floss, H. G.; Froland, W. A.; Lipscomb, J. D.; Williams, P. G.; Morimoto, H., *J. Am. Chem. Soc.* **1992**, *114*, 7561−7562.

10.1021/ic7011217 CCC: $37.00
Published on Web 11/08/2007

bauer studies on samples of the intermediate generated by rapid-freeze quench methods led to the structural assignment of **Q** as a diferryl-di-μ-oxo moiety, the diamond core motif (spectroscopic **Q**),[10,13,14] a conclusion supported by latter XAS,[7] MCD,[15] and ENDOR[16] spectroscopic data and by computational simulations.[17,18] Whereas the kinetic **Q** species is a potent oxidant and has been shown to catalytically oxidize hydrocarbons and arenes,[19−21] a mechanistic linkage between the kinetic **Q** species and the spectroscopic **Q** species (diferryl-di-μ-oxo core) is not as yet unambiguously established.

In addition to utilizing dioxygen as an oxygen-atom source, sMMO is capable of exploiting H_2O_2 via a shunt pathway to oxidize alkane substrates such as methane, propane, and cyclohexane.[22] In this alternative shunt pathway, the presence of dioxygen and the sMMO reductase component are not required for catalysis to occur. Instead, hydrogen peroxide reacts directly with the diferric state of the enzyme to generate a reactive intermediate that oxidatively transforms the alkanes into alcohols. Parallel shunt pathway activity is well established and documented in the family of heme-dependent iron monooxygenases such as cytochrome P450 and related enzymes, although in the latter case, the active site consists of a single iron center.[23]

Except for instances of interspecies warfare (e.g., degradation of plant matter by brown rot fungus,[24] the action of bleomycin,[25] and the adverse environment inside phagocytes,[26]), nature strives to minimize and regulate the *in vivo* production of readily diffusible oxygen-based free radical species. The intracellular presence of the hydroxyl radical is no exception, as its ability to induce cellular apoptosis through the abstraction of hydrogen atoms from any number of important classes of biological molecules in a diffusion-controlled manner originates from the large thermodynamic driving force of HO−H bond (492 kJ mol^{-1}) formation.[27] For this reason, the generation and utilization of peroxides is tightly controlled *in vivo*.[28−30]

Consequently, iron-based monooxygenases appear to have evolved characteristics that support heterolytic cleavage and suppress homolytic cleavage of bound hydroperoxide groups originating from the two-electron metabolic reduction of dioxygen. Homolytic O−O bond scission would generate hydroxyl radicals whose chemistry cannot easily be directed and are thus not particularly useful for performing the highly efficient stereoselective oxidation reactions required in enzyme active sites. sMMO and other monooxygenase enzymes that proceed through an iron hydroperoxide intermediate are thought to cleave the peroxide O−O bond in a heterolytic fashion in the presence of a H^+ donor, resulting in the formal transfer of an oxygen atom to the metal center (i.e., a high-valent iron−oxygen atom species) and the production of 1 equiv of water. Isotopic labeling studies have shown that it is this electrophilic iron-bound oxygen atom that is inserted into the relatively electron rich C−H bond of alkane substrates. Interestingly, in the absence of substrate, it is reported that levels of **Q** in sMMO are depleted via an alternative autodecay pathway ($k = 0.05(1)$ s^{-1} at 4 °C), resulting in the regeneration of the diferric resting state of the enzyme.[12,31] A detailed investigation of this autodecay pathway is currently lacking.

The construction of functional synthetic models of monooxygenase active sites therefore requires, among other chemical features, the development of complexes that induce heterolytic rather than homolytic cleavage of the peroxy O−O bond. The challenges inherent to this requirement are well-documented.[32−36] A parallel approach is to utilize oxygen atom donor (OAD) molecules for the generation of analogous metal-based oxidants. In previous investigations of monooxygenase model systems, (Figure 1), we reported that a binuclear non-heme ferrous complex, $Fe^{II}_2(H_2Hbamb)_2(N\text{-MeIm})_2$ (H_4HBamb = 2,3-bis(2-hydroxybenzamido)-dimethylbutane), **1**, is capable of utilizing either OAD molecules[37,38] or the mechanistic peroxide probe, 2-methyl-1-phenylprop-2-yl hydroperoxide, MPPH,[39] as oxygen-atom sources to effect the oxidation of cyclohexane to cyclohexanol in excess of 300 turnovers and >98% mass balance.[39] GC and GC/MS analysis of the MPPH fragment products

(12) Lee, S. K.; Nesheim, J. C.; Lipscomb, J. D. *J. Biol. Chem.* **1993**, *268*, 21569−21577.
(13) Liu, K. E.; Valentine, A. M.; Wang, D. L.; Huynh, B. H.; Edmondson, D. E.; Salifoglou, A.; Lippard, S. J. *J. Am. Chem. Soc.* **1995**, *117*, 10174−10185.
(14) Liu, K. E.; Wang, D. L.; Huynh, B. H.; Edmondson, D. E.; Salifoglou, A.; Lippard, S. J. *J. Am. Chem. Soc.* **1994**, *116*, 7465−7466.
(15) Skulan, A. J.; Hanson, M. A.; Hsu, H. F.; Que, L.; Solomon, E. I. *J. Am. Chem. Soc.* **2003**, *125*, 7344−7356.
(16) Valentine, A. M.; Tavares, P.; Pereira, A. S.; Davydov, R.; Krebs, C.; Hoffman, B. M.; Edmondson, D. E.; Huynh, B. H.; Lippard, S. J. *J. Am. Chem. Soc.* **1998**, *120*, 2190−2191.
(17) Dunietz, B. D.; Beachy, M. D.; Cao, Y. X.; Whittington, D. A.; Lippard, S. J.; Friesner, R. A. *J. Am. Chem. Soc.* **2000**, *122*, 2828−2839.
(18) Siegbahn, P. E. M. *Inorg. Chem.* **1999**, *38*, 2880−2889.
(19) Green, J.; Dalton, H. *J. Biol. Chem.* **1989**, *264*, 17698−17703.
(20) Prior, S. D.; Dalton, H. *FEMS Microbiol. Lett.* **1985**, *29*, 105−109.
(21) Colby, J.; Stirling, D. I.; Dalton, H. *Biochem. J.* **1977**, *165*, 395−402.
(22) Andersson, K. K.; Froland, W. A.; Lee, S. K.; Lipscomb, J. D. *New J. Chem.* **1991**, *15*, 411−415.
(23) Ortiz de Montellano, P. R. *Cytochrome P-450 : Structure, Mechanism, and Biochemistry*; Plenum Press: New York, 1986.
(24) Hyde, S. M.; Wood, P. M. *Microbiology* **1997**, *143*, 259−266.
(25) Decker, A.; Chow, M. S.; Kemsley, J. N.; Lehnert, N.; Solomon, E. I. *J. Am. Chem. Soc.* **2006**, *128*, 4719−4733.
(26) Saran, M.; Beck-Speier, I.; Fellerhoff, B.; Bauer, G. *Free Radical Biol. Med.* **1999**, *26*, 482−490.
(27) Pogozelski, W. K.; Tullius, T. D. *Chem. Rev.* **1998**, *98*, 1089−1107.
(28) Aebi, H. *Methods Enzymol.* **1984**, *105*, 121−126.
(29) Gajhede, M.; Schuller, D. J.; Henriksen, A.; Smith, A. T.; Poulos, T. L. *Nat. Struct. Mol. Biol.* **1997**, *4*, 1032−1038.
(30) Pelletier, H.; Kraut, J. *Science* **1992**, *258*, 1748−1755.
(31) Valentine, A. M.; Stahl, S. S.; Lippard, S. J. *J. Am. Chem. Soc.* **1999**, *121*, 3876−3887.
(32) Moreira, R. F.; Tshuva, E. Y.; Lippard, S. J. *Inorg. Chem.* **2004**, *43*, 4427−4434.
(33) Nam, W.; Oh, S.-Y.; Lim, M. H.; Choi, M.-H.; Han, S.-Y.; Jhon, G.-J. *Chem. Commun.* **2000**, *18*, 1787−1788.
(34) Nam, W.; Choi, H. J.; Han, H. J.; Cho, S. H.; Lee, H. J.; Han, S.-Y. *Chem. Commun.* **1999**, *4*, 387−388.
(35) MacFaul, P. A.; Ingold, K. U.; Wayner, D. D. M.; Que, L., Jr. *J. Am. Chem. Soc.* **1997**, *119*, 10594−10598.
(36) Wardman, P.; Candeias, L. P. *Radiat. Res.* **1996**, *145*, 523−531.
(37) Mukerjee, S.; Stassinopoulos, A.; Caradonna, J. P. *J. Am. Chem. Soc.* **1997**, *119*, 8097−8098.
(38) Stassinopoulos, A.; Schulte, G.; Papaefthymiou, G. C.; Caradonna, J. P. *J. Am. Chem. Soc.* **1991**, *113*, 8686−8697.
(39) Foster, T. L.; Caradonna, J. P. *J. Am. Chem. Soc.* **2003**, *125*, 3678−3679.

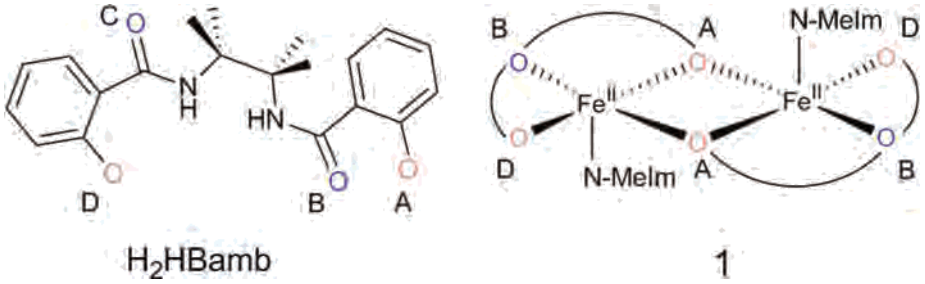

Figure 1. Structure of the ligand and assembled metal complex (**1**).

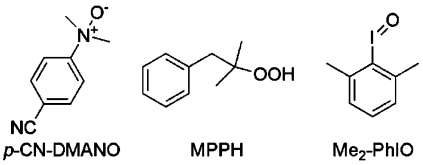

Figure 2. Oxygen atom donor molecules used in this study.

found that, upon the completion of alkane oxidation, the reaction mixture showed the sole presence of heterolytic cleavage products and the absence of any of the possible homolytic induced cleavage products, suggesting a linkage between the iron-based reactive intermediates generated by these two chemically distinct catalytic shunt pathways (i.e., peroxide and OAD). Interestingly, the corresponding binuclear diferric and μ-oxo-diferric complexes derived from the oxidation of **1** were inert as alkane oxidation catalysts in the presence of OAD molecules and were observed to induce homolytic cleavage of MPPH, suggesting reactivity chemistry somewhat different from the active-site chemistry proposed for the family of binuclear iron monooxygenases.[37−39]

In this present study, we report the results of low-temperature, stopped-flow UV−vis spectroscopic studies of the reaction of OAD molecules (Figure 2) with the diferrous non-heme iron **1**. In the absence of substrate, the reaction of [Fe^{II},Fe^{II}] **1** with an OAD molecule proceeds in three steps, assigned as (i) oxygen-atom transfer from the donor molecule to the [Fe^{II},Fe^{II}] core to form a putative [Fe^{II},Fe^{IV}=O] species **2**, (ii) ligand rearrangement of the ferryl terminal oxo species, forming **3**, and (iii) intramolecular oxo-collapse to generate diferric-μ-oxo **4**. Herein, we present evidence for the assignment of each step in this process and discuss potential parallels to key intermediates proposed in the catalytic cycle of sMMO.

Experimental Section

General Experimental Considerations. 1[37] and MPPH[39,40] were synthesized according to previously published procedures. Peroxide activity in MPPH was determined to be >98% by iodometric titration. Prior to use, dimethylformamide (Pharmco, HPLC grade) was processed through a PureSolv solvent purification system from Innovative Technologies. Unstabilized dichloromethane was obtained from Fisher and was distilled over calcium hydride before use. All of the solvents used in air-sensitive work were thoroughly degassed by subjecting them to at least six successive freeze−pump−thaw cycles, after which they were transferred to an inert atmosphere glove box, in which all of the solution preparations were carried out. *m*-Chloroperbenzoic acid (≤77%), diiodopropane (99%), and 2,2′-bipyridine (>99%) were purchased from Sigma Aldrich. *p*-Cyanodimethylaniline (99%) and 50% hydrogen peroxide were purchased from Acros Organics. Molybdenum(VI) oxide (ACS grade) was obtained from Alfa Products. 2,6-Dimethyliodobenzene was purchased from Alfa Aesar.

WARNING! MPPH is an organic peroxide. *The original synthetic procedure calls for the distillation of the extracted peroxide/ether solution, but this resulted in an explosion in our lab*. Gentle removal of ether by blowing a stream of N_2 is recommended as a substitute.

Tetrabutylammonium Octacyanomolybdate(V), (5). Potassium octacyanomolybdate(IV) was prepared as described in *Inorganic Syntheses* and matched the spectroscopic characterizations reported therein.[41] This resulting complex was then oxidized by utilizing a procedure adapted from Withers *et. al*.[42] Potassium octacyanomolybdate(IV) (3.0 g, 6.0mmol) was dissolved in 10 mL water and stirred. Nitric acid (13 mL) was added dropwise to the solution over 15 min, causing evolution of gas. To this mixture, an aqueous solution of tetrabutylammonium bromide (6.2 g, 19mmol) in 25 mL water was added, forming an orange oil. Water (125 mL) was added to the stirring mixture, giving an orange precipitate. The solid was collected by vacuum filtration and washed with 100 mL water and 30 mL diethyl ether. The solid was collected and recrystallized from ethanol/ether, yielding a light-yellow, airy solid. The product was stored in the dark until needed, as it darkens upon prolonged exposure to light. Yield: 3.9 g, 62%. UV−vis: λ_{max} = 392 nm (ϵ = 1380 $M^{-1}cm^{-1}$) (DMF) Electrochemistry: $E_{1/2}$ = −380 mV versus NHE (DMF, 0.5M tetrabutylammonium tetrafluoroborate).

1,1′-Trimethylene-2,2′-dipyridinium Diiodide, (6). This reagent was synthesized following a procedure adapted from Salmon and Hawkridge.[43] 2,2′-Bipyridine (0.5 g, 3.2mmol) and 1,3-diiodopropane (0.95 g, 3.2mmol) were combined in a 25 mL round-bottomed flask. Nitrobenzene (10 mL) and toluene (15 mL) were added to the flask, and a condenser was attached. The solution was heated to reflux for 14 h, producing a bright orange solid, which was collected by vacuum filtration. The solid was dissolved in a hot solution of 15% DMF in ethanol, hot filtered, and crystallized by adding 50 mL ether and placing in the refrigerator overnight. The resulting bright-orange crystals were collected by vacuum filtration. Isolated yield: 0.3 g, 20%. ^{1}H NMR(DMSO-d_6) [2.77(m), 4.44-(m), 5.00(d), 8.50(m), 8.59(t), 9.36 ppm(d)], ^{13}C NMR[30.581, 55.703, 130.954, 131.948, 144.134, 147.411, 147.897 ppm]. Purity >95% by NMR; UV−vis: λ_{max} = 441 nm(ϵ = 120 $M^{-1}cm^{-1}$)

(40) Hiatt, R. R.; Strachan, W. M. J. *J. Org. Chem.* **1963**, *28*, 1893−4.
(41) Van de Poel, J.; Neumann, H. M. *Inorg. Synth.* **1968**, *11*, 53−56.
(42) Withers, J. R.; Li, D. F.; Triplet, J.; Ruschman, C.; Parkin, S.; Wang, G. B.; Yee, G. T.; Holmes, S. M. *Inorg. Chem.* **2006**, *45*, 4307−4309.
(43) Salmon, R. T.; Hawkridge, F. M. *J. Electroanal. Chem.* **1980**, *112*, 253−264.

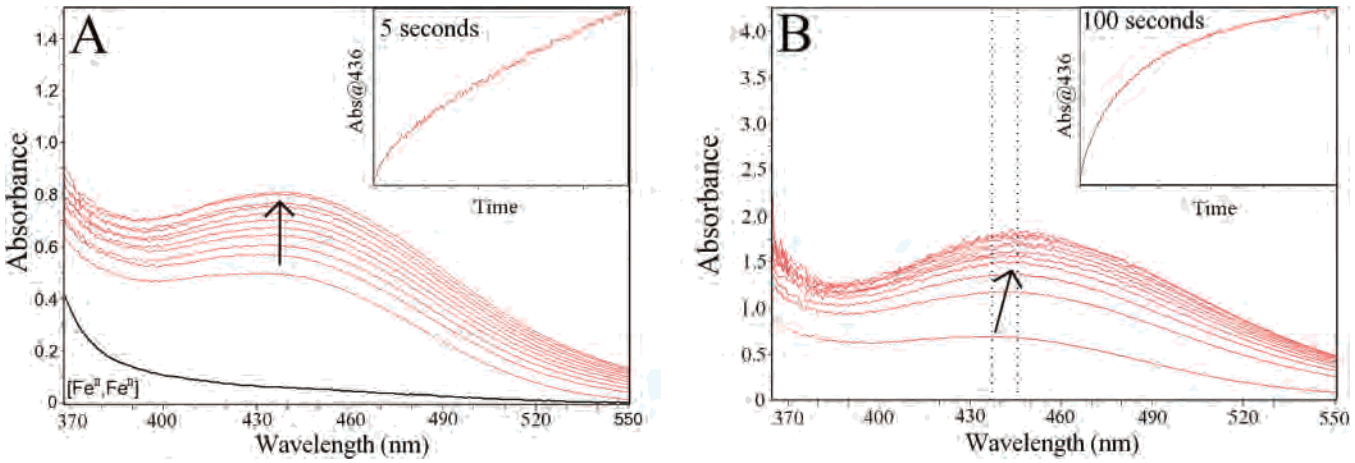

Figure 3. Kinetic plots of (a) buildup of species **2** and **3** (λ_{mx} = 438 nm) at 188 K generated by the reaction of Me_2PhIO (14 mM) with **1** (0.35 mM) over 5 s, superimposed with the spectrum of **1**, with an inset showing an increase in absorbance at 436 nm with time, and (b) a decay of intermediate species to **4** (λ_{max} = 445 nm) over a 100 s time period (with inset).

(DMF). The UV−vis spectrum was consistent with literature values for dipyridinium salts.[44]

2,6-Dimethyliodosylbenzene, (7).[45] Acetic anhydride (13.5 mL, 143mmol) and 50% hydrogen peroxide (1.8 mL, 1.1 g, 65mmol) were added to a 50 mL round-bottomed flask equipped with a magnetic stirbar and stirred at 40 °C for 3.5 h. 2,6-Dimethyliodobenzene (2.5 g, 11 mmol) was then added to the solution dropwise over a 5 min period, with the brown color of 2,6-dimethyliodobenzene disappearing quickly after each drop, accompanied by the evolution of gas. The solution was allowed to stir for 12 h at 45 °C, after which time the solvent was removed by rotary evaporation. The resulting residue was stirred with 10 mL of a 3 M aqueous sodium hydroxide solution for 30 min, forming a yellow solid. The solid was collected by vacuum filtration and stirred with water for 15 min and subsequently with toluene for 30 min, which removed the yellow color, leaving a white solid. The compound was stored at 4 °C when not in use, and a fresh batch was prepared every 3 months. Yield: 0.9 g, 33% yield. ^{1}H NMR(DMF-d_7) [1.71(s), 2.72-(s), 7.19(d), 7.34 ppm(t)]. Greater than 95% activity quantified by reaction with triphenylphosphine followed by NMR measurement of triphenylphosphine oxide.

***p*-Cyanodimethylaniline *N*-Oxide, (8).**[46] *p*-Cyanodimethylaniline (0.93 g, 6.2mmol) was dissolved in 20 mL chloroform in a 50 mL round-bottomed flask and placed in an ice bath. *m*-Chloroperbenzoic acid (1.1 g, 6.2mmol) was dissolved in 20 mL chloroform and added dropwise to the stirring solution of *p*-cyanodimethylaniline. The solution was allowed to stir for 8 h at room temperature, after which the solvent was removed by rotary evaporation. The residue was dissolved in a minimum amount of chloroform and loaded onto a chloroform-packed column of alumina (Brockman, type I basic.) The column was then washed with 50 mL chloroform, and the product was eluted with 25% methanol in chloroform. Removal of the solvent by rotary evaporation yielded a solid that was recrystallized from boiling ethyl acetate, yielding small platelike crystals of the product. Yield: 0.35 g, 35%. ^{1}H NMR($CDCl_3$) [3.58(s), 7.78(d), 8.15 ppm(d)]. Greater than 95% activity quantified by the reaction with triphenylphosphine followed by NMR measurement of triphenylphosphine oxide. All of the NMR spectra were consistent with literature values.[47]

$Fe_2^{III}(H_2Hbamb)_2$(1-methylimidazole)$_2I_2$, (9). A solution of $Fe_2^{II}(H_2Hbamb)_2$(1-methylimidazole)$_2$ (**1**) in DMF (2.8 mg, 2.9μmol in 6.7 mL, 0.43 mM) was prepared in an inert atmosphere glove box. One molar equivalent of iodine (0.72 mg, 2.9μmol) was added by syringe as 0.1 mL of a 29 mM solution in DMF. The solution immediately turned a red-orange color, was swirled to mix the contents, and then slowly changed to a purple color over the next 20 min. UV−vis: λ_{max} = 470 nm (ϵ = 5500 $M^{-1}cm^{-1}$) (DMF). The spectrum was consistent with that previously reported in literature.[37,38]

Fe_2^{III}(μ-O($H_2Hbamb)_2$(1-methylimidazole)$_2$, (4). In an inert atmosphere glove box, $Fe_2^{II}(H_2Hbamb)_2$(1-methylimidazole)$_2$ (**1**) (40 mg, 0.41mmol) was dissolved in 10 mL DMF. To this solution, 2,6-dimethyliodosylbenzene (**7**) (10 mg, 0.040mmol) was added. The solution turned a dark-orange color immediately and was allowed to stir for an additional 15 min. The solution was removed from the glove box, and solvent was removed by rotary evaporation. UV−vis: 445 nm (ϵ = 7000 $M^{-1}cm^{-1}$) (DMF). ^{1}H NMR(DMSO-d_6) [4.22(s), 6.95(s), 7.19(s), 7.32(s), 7.78(s), 12.39 ppm(s)]. IR-(KBr): ν_{as}(Fe−O−Fe) = 840 cm^{-1} The spectra are consistent with those reported in literature.[37,38]

Stopped-Flow Spectroscopy and Data Analysis. Stopped-flow spectroscopy was performed at Tufts University on a Hi-Tech Scientific SF-43 cryogenic double-mixing stopped-flow system operating in single-mixing mode. Low temperatures were maintained through the use of a liquid-nitrogen-cooled heptane bath equipped with a cryostat. To maintain an anaerobic environment, all of the solutions were prepared in an inert atmosphere box and transferred into the stopped-flow spectrometer using gastight syringes. Hi-Tech Scientific IS-2 Rapid Kinetics[48] software package was used to control the instrument and collect data. To ensure adequate time resolution for all of the processes, all of the reactions were monitored at time lengths ranging from 200 ms to 250 s, as appropriate. For each data set, 512 samples were collected in a linear time base. For resolution of exceedingly fast processes, it became necessary to operate the system in single-wavelength mode, which yielded data with an improved signal-to-noise ratio.

(44) Steckhan, E.; Kuwana, T. *Ber. Bunsen-Ges. Phys. Chem.* **1974**, *78*, 253−259.
(45) Sharefkin, J. G.; Saltzman, H. *Anal. Chem.* **1963**, *35*, 1428−31.
(46) Craig, J. C.; Purushot, Kk *J. Org. Chem.* **1970**, *35*, 1721−&.
(47) Ferrer, M.; Sanchez-Baeza, F.; Messeguer, A. *Tetrahedron* **1997**, *53*, 15877−15888.
(48) *Rapid Kinetics Program*, Hi-Tech Scientific: Bradford on Avon, U.K., 1999.

Fits of kinetic data to appropriate models was performed using nonlinear least-squares fitting methods contained in *Specfit/32* version 3.0.36.[49,50]

Results and Discussion

Data Acquisition and Analysis. Under pseudo-first-order conditions, addition of an excess of OAD (20−40-fold) to the diferrous starting complex, **1**, results in the rapid formation of a short-lived intermediate, **2**, that converts to a second intermediate species, **3**, which slowly decays to a final species, **4**, as shown in Figure 3. Kinetic analysis of the reaction's progress across a range of time regimes (i.e., 200 ms, 10 s, 500 s) shows clear triphasic behavior (Figure 4). In the case of the reaction with the OAD *p*-cyanodimethylaniline *N*-oxide (*p*-CN-DMANO), the three processes are amenable to detailed analysis because each successive reaction step is at least 10 times slower than the preceding step.

On the basis of this and other data (*vide infra*), we propose the following mechanism for the reaction of OADs with diferrous **1**, detailed in Scheme 1. In this proposed pathway, the OAD initially reacts with [Fe^{II},Fe^{II}], **1**, to form a Fe^{IV}═O species, **2**. Following the oxidation of the diiron(II) center, the ligand framework rearranges, and the bridging phenolate ligands migrate to a terminal positions, forming **3**. Finally, the Fe^{IV}═O moiety undergoes intramolecular collapse onto the neighboring Fe^{II} center, forming a μ-oxo-Fe^{III}−O−Fe^{III} species, **4**. The stoichiometry of the process is outlined in the eqs 1−3:

$$\mathbf{1} + \text{OAD} \xrightarrow{k_1} \mathbf{2} + [\text{OAD Fragment}] \quad (1)$$

$$\mathbf{2} \xrightarrow{k_2} \mathbf{3} \quad (2)$$

$$\mathbf{3} \xrightarrow{k_3} \mathbf{4} \quad (3)$$

Conversion of 1 to 2. At 185 K, the addition of a 25-fold excess of *p*-CN-DMANO results in the rapid (k_{obs} = 19(2) s^{-1}) formation of an intermediate species with a maximum absorbance at approximately 430 nm ($\epsilon \sim 3000\ M^{-1}\ cm^{-1}$). An exact determination of the maximum absorbance was confounded by the rapidity at which the chromophore developed. The reaction is first order in both iron complex and OAD molecule; excess OAD reagent has no effect on the chromophore's intensity or energy, monitored at 438 nm (Supporting Information). Modeling of the pseudo-first-order reaction with *p*-CN-DMANO gave the best fits, assuming a first-order process (Figure 3), leading us to propose the rate law in eq 4.

$$-\frac{d[1]}{dt} = \frac{d[2]}{dt} = k_{obs}[1] = k_1[1][\text{OAD}] \quad (4)$$

The magnitude of k_1 shows a marked dependence on the nature of the oxidant used, as seen in Table 1. Each OAD reagent contains a different type of X−O bond and, accordingly, reacts with **1** at a dissimilar rate. However, little work has been done to determine the bond dissociation energies of amine *N*-oxides[51] (BDE: $(CH_3)_3N-O$ = 260(5) kJ mol^{-1}) or iodosyl benzene compounds[52] (BDE: 2-iodosobenzoic acid I−O = 265(8) kJ mol^{-1}), and there are no experimentally determined peroxide O−O bond heterolysis energies available for comparison.

Formation of **2** is assigned as a step involving the breakage of the X−O bond of the OAD due to the strong dependence of the rate of formation **2** on the nature of the oxidant (Table 1). Such a dramatic variance in rate would not be expected for simple adduct formation in the absence of significant differential steric interactions. Furthermore, the observed rates are too slow to reflect simple adduct formation; Fe^{II} ligand exchange rates[53] (H_2O exchange $\sim 10^6\ s^{-1}$ at 298 K) are much faster than those observed in the reaction of **1** with OAD molecules. Whereas it is challenging to unambiguously define the precise electronic nature of **2** without more-detailed spectroscopic characterization, the species resulting from the cleavage of an X−O bond of an OAD molecule (Me_2−PhIO, *p*-CN-DMANO, MPPH) and subsequent transfer of the oxygen atom to an Fe^{II} center would suggest that **2** is oxidized by two electrons with respect to **1**, presumably forming an Fe^{IV}═O species. The maximal buildup of intermediate species **2** requires the addition of 1 equiv of an OAD molecule to **1**, and the further addition of OAD has no effect on the chromophore of any subsequent species, establishing a 1:1 stoichiometry (Supporting Information). In addition, the formation of **2** is first order in the OAD molecule and first order in **1**; doubling of the concentration of **1** or *p*-CN-DMANO results in a doubling of the rate (Supporting Information). The hypothesis of an iron-oxo species **2** is further strengthened by the effectively equivalent chromophores (~430 nm) generated by the interaction of [Fe^{II},Fe^{II}] **1** with three different chemical classes of OAD molecules (amine *N*-oxide, substituted iodosyl benzene, alkyl peroxide), which also argues against **2** being a simple Fe^{II}−OAD adduct. Whereas it is plausible that the formal addition of an oxygen atom to diferrous **1** could result in the direct formation of a diferric, μ-oxo moiety, this is not consistent with the subsequent evolution of the resulting complex and the observed kinetic or reactivity data (*vide infra*).[35] Finally, the reaction of **1** with MPPH exclusively forms O−O bond heterolysis products, suggesting that a two-electron oxidation of the initial diiron(II) complex occurs.[39] We therefore currently assign **2** as a ferryl-oxo compound on the basis of these experimental kinetic and mechanistic data.

Conversion of 2 to 3. Following the formation of **2**, a second intermediate species forms with a chromophore centered at 438 nm (ϵ = 4000 $M^{-1}\ cm^{-1}$). At 185 K, the rate of formation of **3** (k_2 = 0.2(1) s^{-1}) is approximately

(49) Maeder, M.; Zuberbuhler, A. D. *Anal. Chem.* **1990**, *62*, 2220−2224.
(50) Binstead, R. A.; Zuberbühler, A. D.; Jung, B. *Specfit/32 Global Analysis System*, version 3.0.36; Spectrum Software Associates: Chapel Hill, N.C., 2004.
(51) Acree, W. E.; Pilcher, G.; da Silva, M. *J. Phys. Chem. Ref. Data* **2005**, *34*, 553−572.
(52) da Silva, M.; Matos, M. A. R.; Ferrao, M.; Amaral, L.; Miranda, M. S.; Acree, W. E.; Pilcher, G. *J. Chem. Thermodyn.* **1999**, *31*, 1551−1559.
(53) Stengle, T. R.; Langford, C. H. *Coord. Chem. Rev.* **1967**, *2*, 349−370.

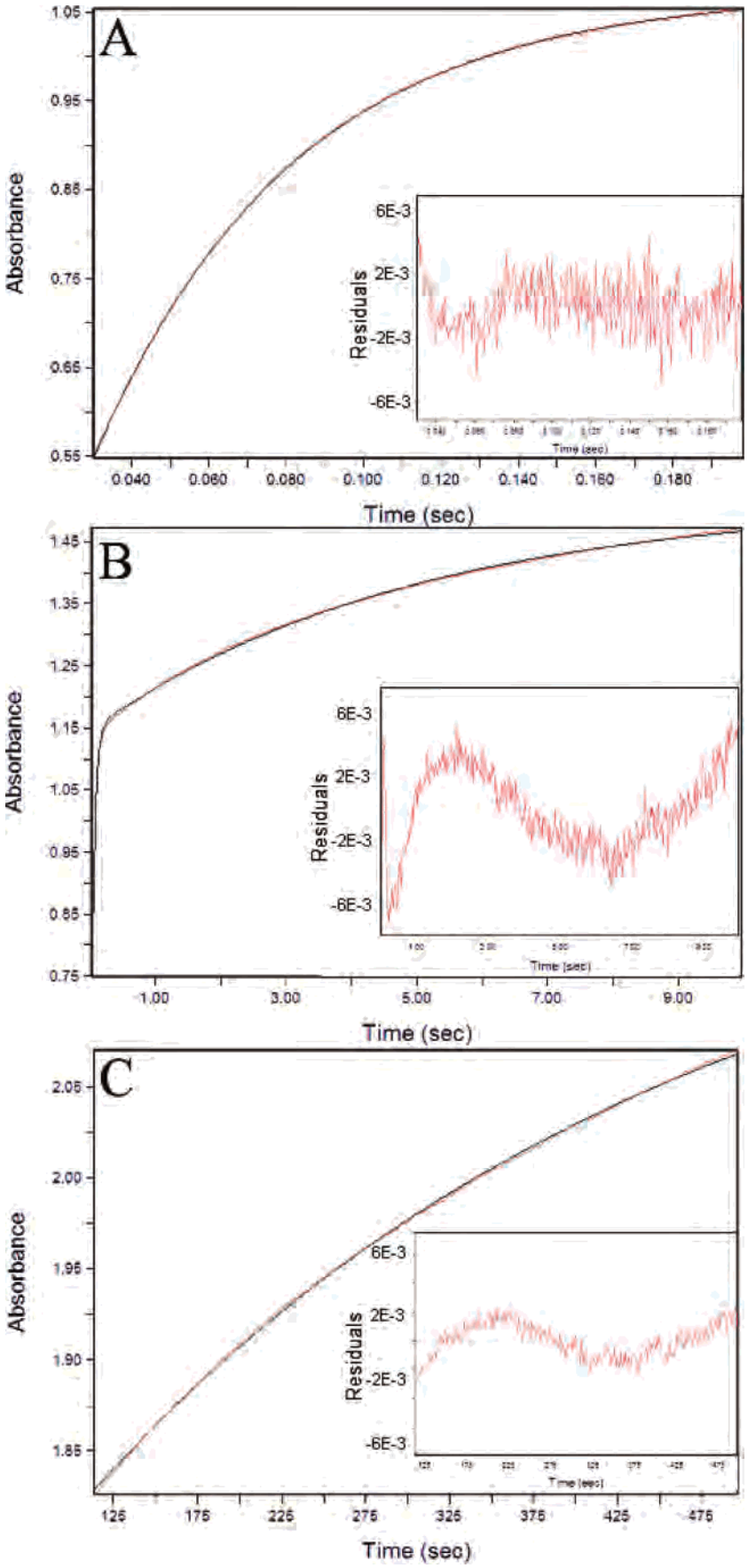

Figure 4. Change in stopped-flow visible absorption at 436 nm versus time upon the reaction of *p*-CN-DMANO (8 mM) and **1** (0.35 mM) at 185 K (red) and kinetic models of data (black) for the (A) 200 ms, (B) 10 s, and (C) 500 s time regimes according to eqs 4, 5, and 8, respectively. Inset: Residuals from fits.

Scheme 1. Proposed Pathway for the Reaction of **1** with OAD[a]

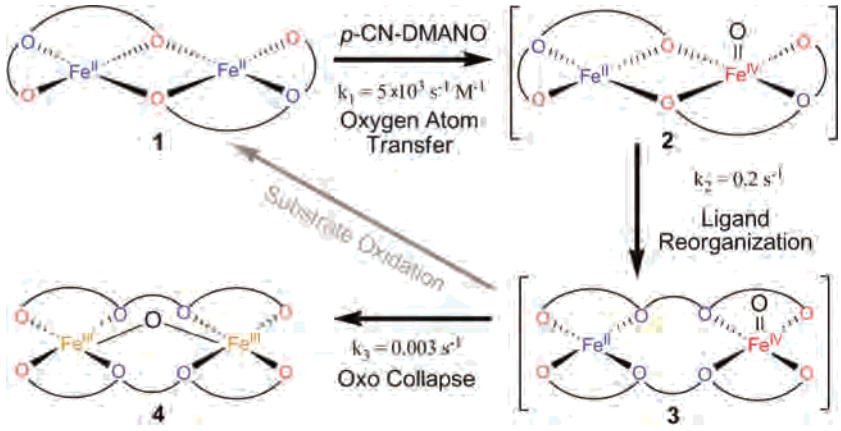

[a] 1-Methylimidazole ligands omitted for clarity. Rates measured at 185 K.

Table 1. Rate Constants for the Reaction of **1** with Different Oxidants at 188 K in 70:30 DCM/DMF

oxidant	k_1 ($s^{-1}M^{-1}$)[a]	k_2 (s^{-1})[b]
p-CN DMANO	$4.7(2) \times 10^3$	0.27(9)
Me_2PhIO	69(5)	0.33(8)
MPPH	10(1)	0.1(1)

[a] According to eq 4. [b] According to eq 5.

100 times slower than the initial buildup of **2**. Modeling the process of **2** → **3** was made possible by including the initial formation of **2** and fixing the initial rate constant to the value obtained in the shorter time regime models. The formation of **3** fits a first-order process, exemplified by eq 5. Unlike the formation of **2**, the process by which **3** forms is unaffected by the nature of the OAD (Table 1). Addition of up to a 10-fold excess of *p*-CN-dimethylaniline (relative to metal complex) has no effect on the magnitude of k_2.

$$-\frac{d[2]}{dt} = \frac{d[3]}{dt} = k_2[2] \qquad (5)$$

The possible identity of **3** included several species, but they can be ruled out as follows, which in turn will lead us to conclude that **3** is a rearrangement product of **2**. First, recall that the assignment of **2** as the X−O bond cleavage product of a 1:1 $[Fe^{II},Fe^{II}]$·O−X adduct to generate a high-valent species was made based, in part, on the sensitivity of the k_1 rate on the X−O bond dissociation energy. These data argue against **2** being a simple $[Fe^{II},Fe^{II}]$·O−X adduct and suggest that the temporal evolution of **2** to **3**, which shows an OAD-independent k_2 rate, does not involve X−O bond cleavage. Second, we can rule out the alternative assignment of **3** as involving a second oxygen-atom transfer reaction from excess OAD to **2**. Although the kinetic competence of **3** in the oxidation of cyclohexane[39] would also be consistent with **3** arising from the reaction of **2** with a second equivalent of OAD, this possibility can be eliminated by the fact that maximal buildup of **3** is achieved upon the addition of 1 equiv of OAD to **1** (Supporting Information), as well as the insensitivity of the magnitude of k_2 on the nature of the X−O bond (Table 1). Third, we can also rule out the assignment of **3** arising from interactions between **2** and excess OAD (**2**·OAD adduct) owing to the 1:1 OAD/**1** stoichiometry of the reaction ultimately forming **3**. Additionally, an adduct of **2** with a deoxygenated OAD fragment can be ruled out due to the insensitivity of k_2 to the exogenous addition of up to a 10-fold excess of *p*-cyanodimethylaniline to the reaction mixture in experiments, utilizing *p*-CN-DMANO as the OAD.

Finally, we considered the possibility of **2** breaking apart into two monomeric species subsequent to the OAD transfer step, but this, too, was ruled out for the following reasons. It is known from mass-spectrometric data that either one- or two-electron chemical oxidation of **1** results in dimeric $[Fe^{II},Fe^{III}]$ and $[Fe^{III},Fe^{III}]$ complexes, respectively.[38] Also, if **2** fragments into two monomeric species following oxygen-atom transfer, it is likely that the result would be an Fe^{IV}═O and Fe^{II} species, with the latter species expected to react with a second equivalent of OAD molecule. Because no observed process subsequent to the initial oxygen-atom transfer step demonstrates any sensitivity to the nature or concentration of the OAD molecule (*vide infra*), this possibility seems unlikely. Additionally, cleavage into two Fe^{II} monomeric species followed by recombination to form a μ-oxo-diiron(III) compound can be ruled out in light of the catalytic reactivity and observed turnover rate of **1** in the presence of OAD and substrate (i.e., inactivation of this complex toward catalysis would occur far too rapidly at room temperature to allow for oxidation of the substrate).[39,54]

We propose, then, that intermediate **3** is a ligand-rearranged form of intermediate **2**. It is known from electrochemical, EPR, and crystallographic studies that upon oxidation, the core of **1** undergoes rearrangement. The crystal structures of reduced[38] and oxidized[55] analogues of a related ligand system of **1** (*o*-phenylene diamine vs 2,3-diamino-2,3-dimethyl butane (**1**) ligand backbone) are shown in Figure 5. In the initial diferrous state (part A of Figure 5), each Fe^{II} center is bridged by two phenolate oxygen atoms from two different ligands (Figure 1). In addition to these two bridging phenolate atoms, each Fe^{II} center is coordinated to an amide

(54) Stassinopoulos, A.; Caradonna, J. P. *J. Am. Chem. Soc.* **1990**, *112*, 7071−7073.
(55) Cappillino, P.; Rowe, G.; Tarves, P.; Rogge, C.; Spuches, A. M.; Stassinopoulos, A.; Lo, W.; Armstrong, W.; Caradonna, J. P., manuscript submitted, 2007.

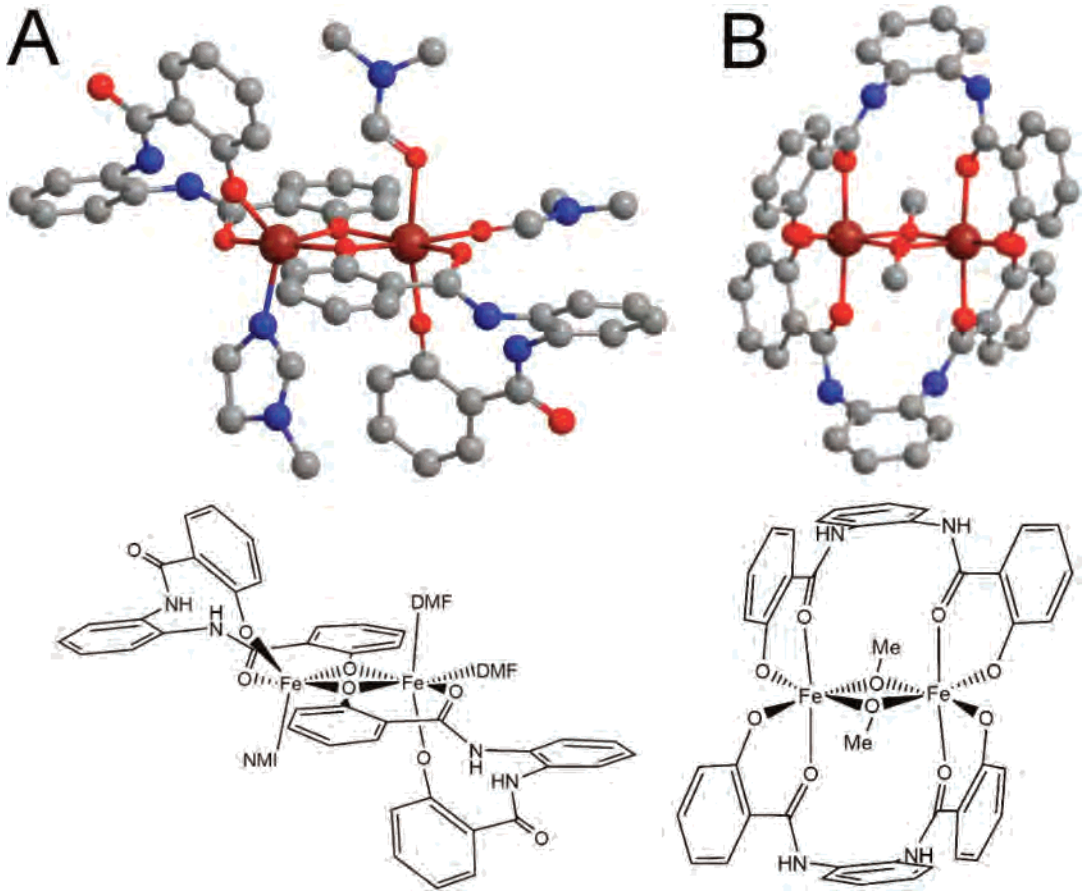

Figure 5. Crystal Structures of (a) a diferrous complex closely related to **1** from ref 38 and (b) a diferric, dim ethoxy complex showing the ligand rearrangement that occurs upon oxidation from ref 55. NMI = 1-methylimidazole; DMF = dimethylformamide.

carbonyl oxygen atom and to an additional monodentate phenolate oxygen atom. The binding of an exogenous *N*-MeIm ligand completes the NO_4 distorted trigonal-bipyramidal iron coordination sphere. The crystal structure (part B of Figure 5) of the oxidized form of the complex (generated either chemically or electrochemically) shows that the ligand framework has undergone a reorganization with respect to that arrangement observed in the diferrous compound, with the bridging phenolate groups shifted to terminal positions and the phenolate and amide carbonyl atoms of each half of the ligand binding to a different Fe^{III} center. The presence two bridging methoxy groups originating from the methanol solvent complete the distorted-octahedral geometry of each Fe^{III} center. It can be inferred that at some point in the oxidative process, the ligand framework must reorganize to give the conformation seen in part B of Figure 5. This reorganization process is a broad-based phenomenon and is conserved across all crystallographically characterized structurally analogous diiron complexes based on the bis-phenoxy-bis-amido ligand framework (ligand backbones include benzene, propane, butane, and pentane) present in **1**.[55]

One-Electron Oxidation Experiments. A series of one-electron oxidation kinetic experiments were designed and performed to examine whether the known ligand-reorganization process occurs according to a kinetic scheme consistent with the observed conversion of **1** → **2** → **3**. Previous electrochemical studies suggested that the one-electron oxidation of **1** ($[Fe^{II},Fe^{II}] \rightarrow [Fe^{II},Fe^{III}]$) conforms to an EC mechanism, characterized by the scan-rate dependence of the cyclic voltammagram.[38] The dependence of ΔE_p versus scan rate for the $[Fe^{II},Fe^{II}]/[Fe^{II},Fe^{III}]$ couple was attributed to kinetic effects (it was independent of complex concentration, the addition of 10 equiv of *N*-MeIm, or the addition of 1−3 equiv of NEt_3), consistent with an intramolecular event that was assigned as a structural reorganization. Whereas the resulting $[Fe^{II},Fe^{III}]$ mixed valence complex can be further oxidized by one electron to an $[Fe^{III},Fe^{III}]$ complex (both $[Fe^{II},Fe^{III}]$ and $[Fe^{III},Fe^{III}]$ dimeric complexes show g_{eff} = 4.3 EPR signals indicating uncoupled Fe^{n+} centers), the cyclic voltammetry data show effectively electrochemically reversible behavior (ΔE_p of 70 mV with no scan-rate dependence) for this latter $[Fe^{II},Fe^{III}]/[Fe^{III},Fe^{III}]$ couple. These data suggest that the second oxidation of the $[Fe^{II},Fe^{III}]$ to the $[Fe^{III},Fe^{III}]$ complex is not accompanied by a conformational change. Direct structural evidence for the reorganization process following the chemical or air oxidation of $[Fe^{II},Fe^{II}]$ **1** to the $[Fe^{III},Fe^{III}]$ complex in MeOH is also available from single-crystal X-ray diffraction studies (Figure 5), where differences in the way the ligand binds to the $[Fe^{II},Fe^{II}]$ and $[Fe^{III},Fe^{III}]$ cores are evident.[55]

Knowledge of the existence of this reorganization phenomenon encouraged us to measure the rate of the intramolecular rearrangement process. Consequently, the kinetics of

Table 2. One-Electron Oxidation Reactions and Ligand Reorganization at 188 K

oxidant	$E_{1/2}$ versus NHE (mV)	k_1 (s^{-1} M^{-1})	k_2 (s^{-1})
$[Mo(CN)_8]^{-III}$	−380[a]	$5.2(5) \times 10^4$	0.75(10)
viologen	−560[b]	$2.4(6) \times 10^2$	0.74(10)
$[Fe^{III},Fe^{III}]$	−310[a]	$4.3(5) \times 10^2$	1.0(1)

[a] Measured in DMF and referenced to Fc/Fc^+ (0.4 vs NHE). [b] Ref 43.

Scheme 2. Chemical Equations Used to Model the Reaction of **1** and One-Electron Oxidants

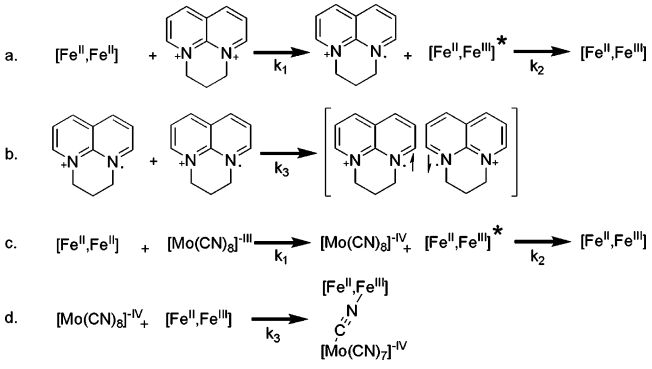

the initial one-electron $[Fe^{II},Fe^{II}] \rightarrow [Fe^{II},Fe^{III}]$ process were followed by stopped-flow spectroscopy by observing the chromophore arising from the phenolate-to-Fe(III) LMCT band in the visible spectrum (436 nm, $\epsilon = 5500$ $M^{-1}cm^{-1}$) to determine the rate constants of both the initial oxidation step and subsequent conformational change. To facilitate this set of experiments, three different one-electron oxidants were carefully selected according to their reduction potentials (Table 2) such that each oxidant was capable of effecting the first one-electron oxidation, but incapable of causing the second one-electron oxidation to the $[Fe^{III},Fe^{III}]$ compound. In addition to the two traditional oxidants (octacyanomolybdate(V) and viologen), the $[Fe^{III},Fe^{III}]$ complex itself was used as a one-electron oxidant, as it will comproportionate ($K_{com} = 1.7 \times 10^4$) with the $[Fe^{II},Fe^{II}]$ compound, **1**, to generate 2 equiv of the mixed-valent $[Fe^{II},Fe^{III}]$ complex.

Irrespective of the oxidant employed, each process conformed to a fast initial electron-transfer step followed by a slower reorganization step that could be modeled by eqs 6 and 7. In the cases of viologen and octacyanomolybdate(V), a subsequent, third step was observed. One-electron reduced viologens are reported to form spin-paired dimers in polar solvents at low temperatures. Further evidence for this process arises from the observed hypsochromic shift in the reduced viologen chromophore, which is known to accompany dimerization (part b of Scheme 2).[56,57] Octacyanomolybdate(IV) is similarly known to form adducts with metal complexes through the formation of CN^- bridges, and the observed third step is assigned as such (part d of Scheme 2).[58] Kinetic schemes used in fitting these subsequent processes are shown in Scheme 2. Kinetic fits to models are shown in Figures S4−S6 in the Supporting Information.

$$-\frac{d[Fe^{II},Fe^{II}]}{dt} = \frac{d[Fe^{II},Fe^{III}]^*}{dt} = k[Fe^{II},Fe^{II}][\text{Oxidant}] \quad (6)$$

$$-\frac{d[Fe^{II},Fe^{III}]^*}{dt} = \frac{d[Fe^{II},Fe^{III}]}{dt} = k[Fe^{II},Fe^{III}]^* \quad (7)$$

Like the oxygen-atom transfer experiments, all of the one-electron oxidation processes occur in two steps: a fast, oxidant-dependent electron-transfer step followed by a slower, oxidant-independent step assigned to ligand reorganization. This model is consistent with what we observe for the conversion of **1** → **2** → **3**. The rapid one-electron oxidation of **1** at 188 K results in the generation of a short-lived species ($[Fe^{II}, Fe^{III}]^*$) that rearranges at an oxidant-independent rate ($k \approx 0.9(1)$ s^{-1}) to give the final rearranged $[Fe^{II},Fe^{III}]$ compound. This one-electron induced reorganization rate is not significantly different from the proposed reorganization rate measured in the reaction of **1** with OAD molecules at the same temperature ($k_2 = 0.2(1)$ s^{-1}), taking into consideration the proposed different oxidation states involved in the unreorganized dimers ($[Fe^{II}, Fe^{III}]$ vs $[Fe^{II}, Fe^{IV}{=}O]$).

In an attempt to preclude the presence of a third (adduct formation) step in the kinetic process, diferrous **1** ($[Fe^{II}, Fe^{II}]$) was combined with diferric complex ($[Fe^{III}, Fe^{III}]$) in a comproportionation reaction to generate 2 equiv of the mixed-valence complex ($[Fe^{II}, Fe^{III}]$). Unlike the other one-electron oxidants, this reaction is not expected to produce any byproducts. A proposed mechanism for this reaction is shown in Scheme 3. Because the starting diferric oxidant complex is already rearranged, it should, upon comproportionation, already adopt the rearranged mixed-valence complex structure. However, upon rapid oxidation, the diferrous complex forms an unstable intermediate ($[Fe^{II}, Fe^{III}]^*$) that must then rearrange to yield the final mixed-valence compound. Spectroscopically, this should manifest itself as two-phase behavior in the absorbance at the chromophore for $[Fe^{II}, Fe^{III}]$. Simulations of the collected kinetic data fit well to this scheme, further supporting the hypothesis of a structural reorganization for the k_2 process (Supporting Information).

Taking these experimental observations together, we propose that **3** represents a reorganized species whose ligand arrangement process is comparable to that of the one-electron reorganized complexes (and two-electron oxidized structure) previously discussed. Although the formal core oxidation states resulting after the interaction of **1** with an oxygen atom must be higher than those generated by the simple one-electron oxidation processes, we nonetheless assign the k_2 process as a similar structural rearrangement.

Conversion of 3 to 4. With time, **3** quantitatively converts to a stable species (**4**) characterized by a more intense, bathochromically shifted chromophore (445 nm, $\epsilon = 8000$

(56) Evans, A. G.; Evans, J. C.; Baker, M. W. *J. Chem. Soc., Perkin Trans. 2* **1977**, *13*, 1787−1789.
(57) Monk, P. M. S.; Hodgkinson, N. M.; Ramzan, S. A. *Dyes Pigm.* **1999**, *43*, 207−217.
(58) Sieklucka, B.; Podgajny, R.; Przychodzen, P.; Korzeniak, T. *Coord. Chem. Rev.* **2005**, *249*, 2203−2221.

Scheme 3. Proposed Mechanism for Comproportionation

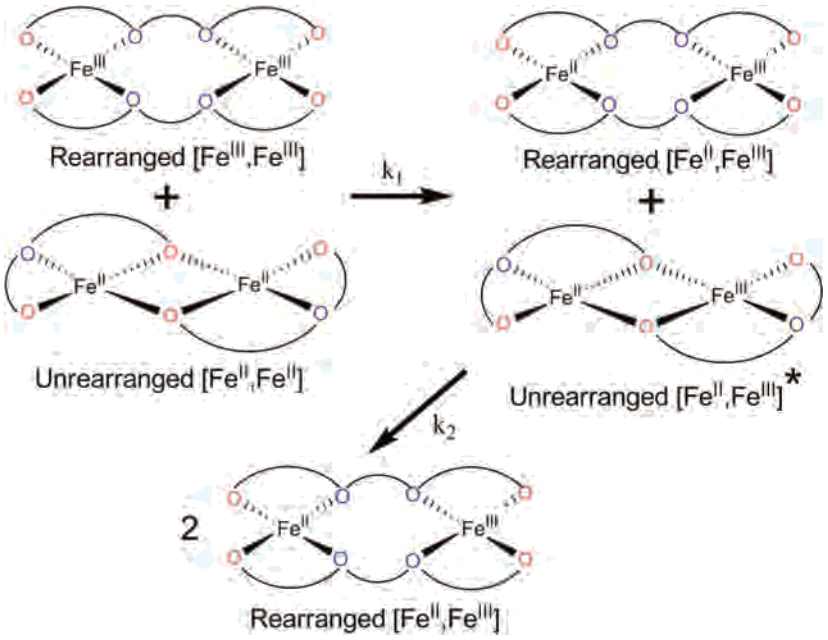

M^{-1} cm^{-1}). The final process fits to a first-order model (eq 8, part c of Figure 4) and results in a compound that has been identified as a diferric μ-oxo species. At 185 K, the rate of formation of **4** is slower than those of the other two processes ($k_3 = 0.003(1)$ s^{-1}). The rate of formation of **4** is unaffected by exposure to broad-spectrum ultraviolet light, which is reported to accelerate the decay of high-valent iron species in enzymatic systems.[31]

$$-\frac{d[3]}{dt} = \frac{d[4]}{dt} = k_3[3] \qquad (8)$$

4 is air stable and is spectroscopically identical to an authentic μ-oxo compound independently produced by alternative synthetic means. Chemical oxidation of diferrous **1** to the [Fe^{III}, Fe^{III}] form followed by the addition of a stoichiometric amount of water and base results in a compound identical in all aspects to **4**. The infrared spectrum of **4** contains an asymmetric Fe−O−Fe stretch ($\nu_{as} = 840$ cm^{-1}) that is sensitive to ^{18}O labeling (Fe−^{18}O−Fe stretch ($\nu_{as} = 805$ cm^{-1}), generated by the reaction of ^{18}O-labeled iodosylbenzene with **1**, indicating that the bridging μ-oxo group originates from the OAD molecule. Additionally, **4** is diamagnetic, allowing for analysis by ^1H NMR spectroscopy (Figure S7 in the Supporting Information), indicating that the two Fe(III) centers are antiferromagnetically coupled through the oxo-bridge. The conversion of a terminal ferryl-oxo species to a diferric μ-oxo compound conversion is unsurprising in light of the stability and ubiquity of diferric μ-oxo compounds.[59,60] This conclusion is consistent with the complete inhibition of OAD-induced catalytic oxidation of the substrate upon the formation of the diferric μ-oxo compound (i.e., addition of OAD or peroxide to **4** does not result in the formation of a new, high-valent species).[39]

(59) Kurtz, D. M. *Chem. Rev.* **1990**, *90*, 585−606.
(60) Murray, K. S. *Coord. Chem. Rev.* **1974**, *12*, 1−35.

Table 3. Activation Parameters for Reactions with *p*-CN-DMANO[a]

reaction	$\Delta H^{\ddagger}$ (kJ/mol)	$\Delta S^{\ddagger}$ (J/K·mol)	$\Delta G^{\ddagger}_{188K}$ (kJ/mol)
1 → **2**	36(4)	21(12)	33(5)
2 → **3**	49(4)	15(4)	46(4)
3 → **4**	50(5)	7(4)	48(6)

[a] All of the reaction trials were performed under pseudo-first-order conditions.

Activation Parameters. Acquisition of kinetic data for the reaction of **1** with *p*-CN-DMANO over a range of temperatures (185−206 K) allowed for the determination of activation parameters of the three processes via Eyring analysis. At temperatures exceeding 206 K, reaction rates become too great ($k_1 > 800$ s^{-1}) for adequate resolution of subsequent processes, and, as such, are not included in this analysis. The results are shown in Table 3. Each successive process has a higher enthalpy of activation and a lower entropy of activation than those preceding it. Taken together, this means that rate crossover will never occur for any two processes (i.e., the rate of each process will always be slower than the one before it, regardless of temperature). This fact lends credence to the low-temperature studies being relevant to the catalysis that occurs at room temperature. If the relative rate for the intramolecular collapse of **3** → **4** becomes much faster than the rate for the conversion of **2** → **3** at higher temperatures, we would expect to observe a strongly negative effect on the catalytic abilities of this system, as inert **4** would form too quickly after the formation of **3**, generating a catalytically inactive compound. This conclusion is further supported by the effective absence of **4** during the catalytic oxidation of cyclohexane to cyclohexanol, because **4** is known to induce solely homolytic cleavage of MPPH, and only heterolytic cleavage products are observed.[39]

The activation parameters for the conversion of **1** → **2** are consistent with predictions of a dissociative transition state, with a moderately high activation enthalpy and entropy. This provides further evidence that the rate-limiting step in

the conversion of **1** → **2** is not the binding of OAD to the metal complex, as this would likely yield a large, negative entropy of activation. In light of the other kinetic data, the moderate, positive entropy of activation for the conversion of **1** → **2** suggests that the transition-state complex consists of **1** and the molecule of OAD already ligated, with its X−O bond in the process of breaking.

The subsequent two processes (k_2 and k_3) are assigned as intramolecular rearrangement processes, and their strikingly similar activation parameters attest to that presumption. As the activation entropies for the processes forming **3** and **4** are relatively small, it unlikely that the complex breaks apart into two monomeric species at any point in the reaction process. It should be noted that rigorous comparison of the three sets of activation parameters is not possible, save at some arbitrary concentration, due to the different standard states (i.e., their different units) of the bimolecular k_1 process and the unimolecular k_2 and k_3 processes.

The observation of phenolate bridges between the two ferrous centers that later break upon oxidation of the diiron core suggests an intriguing hypothesis for a role of the second Fe^{II} center during formation of the reactive intermediate. Our current kinetic-based model suggests that the initial step in the interaction of an OAD molecule with the diferrous core of **1** involves the formal two-electron oxidation of one ferrous center to form **2** prior to the known structural reorganization of the complex to form **3**. It is now interesting to consider whether the increased energy of a reactive intermediate such as **2** or the energy barrier to its formation is stabilized in part by the presence of electron density from the neighboring coupled ferrous iron through the two phenolate bridges. Any potential stabilization of **2** is expected to diminish upon the conversion of **2** → **3**, as a consequence of the structural rearrangement that isolates the Fe^{IV}═O reactive center, thereby increasing its relative position in the overall energy landscape. A potential parallel in chemistry may be drawn to the carboxylate shift that occurs in the catalytic cycle of binuclear non-heme iron enzymes, in which a bridging carboxylate ligand that exists in the reduced, diferrous form of the enzyme shifts to a terminal position upon oxidation to the diferric and other oxidized states along the catalytic cycle.[61−64] It has been proposed that this shift facilitates dioxygen binding to the iron centers in the enzymatic systems but may have other effects as well.[61,65] Detailed spectroscopic characterizations and computational simulations of **1** and **4**, along with highly reactive species **2** and **3**, are currently underway.

Finally, the conversion of **3** to the inert μ-oxo-[Fe^{III},Fe^{III}] dimer, **4**, results in a loss of catalytic activity, thereby implying an upper bound on the free energy of activation (48 kJ mol^{-1} at 188 K) corresponding to any substrate oxidation process. The direct measurement of these values for a variety of alkane substrates by temperature-dependent stopped-flow spectroscopy is under investigation. This characteristic also has an effect on the lifetime of the catalyst in solution when oxidizing various substrates, namely that the presence of substrate does not necessarily preclude the formation of **4** and that the catalytic efficiency is intrinsically linked to the barrier to substrate oxidation.[39]

Table 4. UV−Vis Features of Fe(IV)-Oxo Complexes

compound	λ_{max} (nm)	ref
Fe(IV)(O) cyclam-acetato	676	74
Fe(IV)(O) TMC	820	73
Fe(IV)(O) TPA	724	72
Fe(IV)(O) N4Py	695, 800(sh)	70
Fe(IV)(O) Bn-tpen	739, 900(sh)	70
Fe(IV)(O) Me-tppn	742	71
Fe(IV)(O) Me-tpen	756	71
Fe(IV)(O) BPMCN	753	69
Fe(IV)(O) TMCS	460, 570, 850, 1050	68
Fe(IV)(O) TAPH	750	66
Fe(IV)(O) TAPM	890	66
Fe(IV)(O) Me_3-TPA	770, 890(sh), 935(sh)	67
Fe(IV)(O) QBPA	775, 895(sh), 950(sh)	67
$TauD_J$ Fe(IV)(O)	318	79
Fe(IV)-O−Fe(III) $(Ar^{Tol}COO^-)_4$	∼670	75
Fe(IV)-O−Fe(III) $(TACN)_2$	566, 912	76
Fe(IV)-O−Fe(III) Me_3-TPA	490, 640	77
Fe(IV)(O),Fe(II) H_2Hbamb (**3**)	438	this work
$sMMO_Q$ (*M. trichosporium*)	430	10
$sMMO_Q$ (*M. capsulatus*)	420	13

Comparison to Other Systems. Spectroscopic characterizations of other high-valent iron-oxo compounds, both mononuclear (Fe^{IV}═O)[66−74] and binuclear (Fe^{III}−O−Fe^{IV}),[75−77] are reported in the literature. The UV−vis spectroscopic data for selected iron-oxo compounds are reported in Table 4. For each of the synthetic mononuclear species, there is a predominance of low-energy absorption transitions, spanning

(61) Whittington, D. A.; Lippard, S. J. *J. Am. Chem. Soc.* **2001**, *123*, 827−838.
(62) Gherman, B. F.; Baik, M. H.; Lippard, S. J.; Friesner, R. A. *J. Am. Chem. Soc.* **2004**, *126*, 2978−2990.
(63) Moche, M.; Shanklin, J.; Ghoshal, A.; Lindqvist, Y. *J. Biol. Chem.* **2003**, *278*, 25072−25080.
(64) Krebs, C.; Davydov, R.; Baldwin, J.; Hoffman, B. M.; Bollinger, J. M.; Huynh, B. H. *J. Am. Chem. Soc.* **2000**, *122*, 5327−5336.
(65) Dunietz, B. D.; Beachy, M. D.; Cao, Y.; Whittington, D. A.; Lippard, S. J.; Friesner, R. A. *J. Am. Chem. Soc.* **2000**, *122*, 2828−2839.
(66) Suh, Y.; Seo, M. S.; Kim, K. M.; Kim, Y. S.; Jang, H. G.; Tosha, T.; Kitagawa, T.; Kim, J.; Nam, W. *J. Inorg. Biochem.* **2006**, *100*, 627−633.
(67) Paine, T. K.; Costas, M.; Kaizer, J.; Que, L., Jr. *J. Biol. Inorg. Chem.* **2006**, *11*, 272−276.
(68) Bukowski, M. R.; Koehntop, K. D.; Stubna, A.; Bominaar, E. L.; Halfen, J. A.; Muenck, E.; Nam, W.; Que, L., Jr. *Science* **2005**, *310*, 1000−1002.
(69) Jensen, M. P.; Costas, M.; Ho, R. Y. N.; Kaizer, J.; Payeras, A. M.; Muenck, E.; Que, L., Jr.; Rohde, J.-U.; Stubna, A. *J. Am. Chem. Soc.* **2005**, *127*, 10512−10525.
(70) Kaizer, J.; Klinker, E. J.; Oh, N. Y.; Rohde, J.-U.; Song, W. J.; Stubna, A.; Kim, J.; Muenck, E.; Nam, W.; Que, L., Jr. *J. Am. Chem. Soc.* **2004**, *126*, 472−473.
(71) Balland, V.; Charlot, M.-F.; Banse, F.; Girerd, J.-J.; Mattioli, T. A.; Bill, E.; Bartoli, J.-F.; Battioni, P.; Mansuy, D. *Eur. J. Inorg. Chem.* **2004**, *2*, 301−308.
(72) Lim, M. H.; Rohde, J.-U.; Stubna, A.; Bukowski, M. R.; Costas, M.; Ho, R. Y. N.; Munck, E.; Nam, W.; Que, L., Jr. *Proc. Natl. Acad. Sci. U.S.A.* **2003**, *100*, 3665−3670.
(73) Rohde, J.-U.; In, J.-H.; Lim, M. H.; Brennessel, W. W.; Bukowski, M. R.; Stubna, A.; Muenck, E.; Nam, W.; Que, L., Jr. *Science* **2003**, *299*, 1037−1039.
(74) Grapperhaus, C. A.; Mienert, B.; Bill, E.; Weyhermueller, T.; Wieghardt, K. *Inorg. Chem.* **2000**, *39*, 5306−5317.
(75) Lee, D.; Bois, J. D.; Petasis, D.; Hendrich, M. P.; Krebs, C.; Huynh, B. H.; Lippard, S. J. *J. Am. Chem. Soc.* **1999**, *121*, 9893−9894.
(76) Slep, L. D.; Mijovilovich, A.; Meyer-Klaucke, W.; Weyhermuller, T.; Bill, E.; Bothe, E.; Neese, F.; Wieghardt, K. *J. Am. Chem. Soc.* **2003**, *125*, 15554−15570.
(77) MacMurdo, V. L.; Zheng, H.; Que, L. *Inorg. Chem.* **2000**, *39*, 2254−2255.

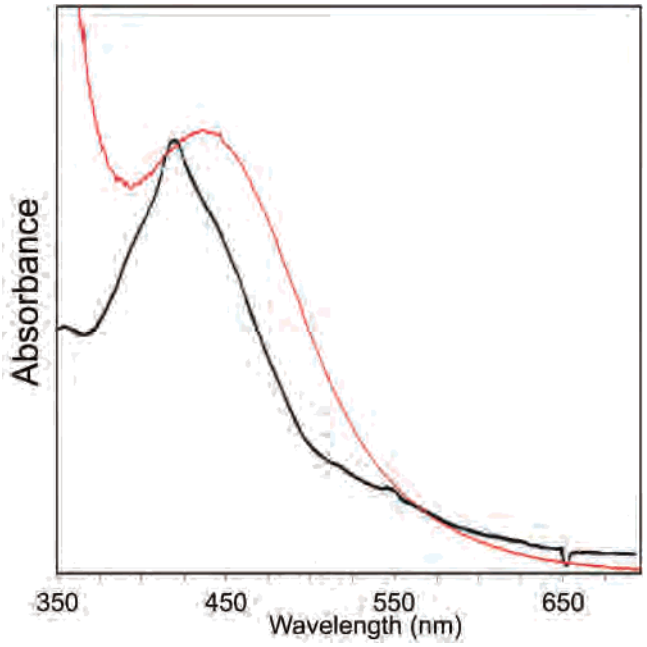

Figure 6. Comparison of oxidizing intermediates of MMO_Q (black line), adapted from ref 13, and **3** (red line). Absorbance levels normalized for comparison.

the range of 600−1000 nm. In addition, most of the spectroscopically characterized iron-oxo complexes are relatively stable at low temperatures, some even persisting long enough to allow for the growth of diffraction-quality crystals.[73,78] In light of the stability of these compounds, it is not particularly surprising that they exhibit diminished reactivity toward alkane substrates but readily oxidize more-reducing substrates like phosphines and sulfides.[70] Biological mononuclear iron-oxo species, such as the high-spin Fe^{IV}═O intermediate species observed in $TauD_J$,[79] possess UV−vis chromophores with substantially higher energy, in the range of 300−350 nm, than those transitions reported for the low-spin synthetic model complexes. Finally, whereas comparisons of the chromophores associated with **2** and **3** and the mononuclear $TauD_J$ Fe^{IV}═O intermediate species are only marginally better, the close parallels between the electronic spectra of **2** and **3** and the high-valent diiron(IV)-oxo core of kinetic **Q**[10,13] (Table 4, Figure 6) are noteworthy. Again, agreement between the chromophores reported for the kinetic **Q** of *M. trichosporium* (430 nm),[10] *M. capsulatus* (420 nm),[13] and **2** and **3** (438 nm) versus synthetic [Fe^{III},-Fe^{IV}] dimers (>490 nm) are marginal (Table 4). One common theme in many of the characterized iron-oxo model compounds is that their coordination spheres are nitrogen-rich. The nitrogen environment may play a part in stabilizing the high oxidation state of the iron, but in doing so, may also lower the reactivity toward substrates.

In contrast, **1** possesses an oxygen-rich ligand set that yields a high-valent intermediate with a single chromophore in the visible region centered at 438 nm. We believe that this may be a factor affecting the electronic structure and, hence, activity of our catalytic system, which has been shown to heterolytically cleave MPPH and oxidize cyclohexane to its corresponding alcohol in excess of 300 turnovers.[39] No data are currently available; however, to differentiate between the ability of **2** or **3** to support alkane oxidation chemistry, only that a reactive intermediate with an absorption near 438 nm is kinetically competent.

Scheme 4. Decay Pathways of **3** and Proposed MMO_Q

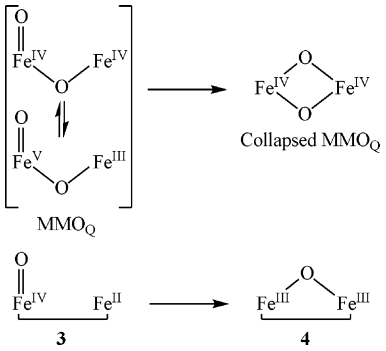

Potential Biological Relevance. The observation that the formal ferryl-oxo **3** undergoes autoconversion to a catalytically inert μ-oxo-diferric compound is particularly interesting in light of potential parallels that can be drawn to the proposed catalytic intermediate of sMMO, **Q**. Spectroscopic **Q** has been assigned as a diferryl, di-μ-oxo species on the basis of XAS and Mössbauer spectroscopic studies.[7] UV−vis-based stopped-flow spectroscopic analyses of **Q** show a kinetically competent species with $\lambda_{max} \approx 420$ nm,[12,13] not significantly different from the 438 nm chromophore (30% DMF in CH_2Cl_2) found for **3** (Figure 6). We submit that **1** represents a credible functional analogue of the reduced active site of sMMO.[39] Even though **3** ([Fe^{IV}═O,Fe^{II}]) is two electron equivalents reduced from the diferryl core of **Q**, **3** is a plausible model for the active oxidant of sMMO on the basis of (i) the reported alkane oxidation chemistry supported by **1**,[37,39] (ii) the ability of **1** to induce heterolytic cleavage of MPPH, (iii) the equivalence of the electronic spectra of the intermediates generated by either MPPH or a variety of OAD molecules, and (iv) the close similarity of the electronic spectra of **3** and **Q** of sMMO. Furthermore, the facile first-order conversion of intermediate **3** to the μ-oxo-[Fe^{III},Fe^{III}] **4** raises the possibility of parallel intermediate conversion processes in the active site of sMMO (Scheme 4). The implication that a comparable first-order conversion of a ferryl terminal oxo moiety to a bridging μ-oxo group in the oxidized diiron sMMO active-site core would potentially generate a diferryl, di-μ-oxo species is worthy of further consideration and experimental investigation by the biophysical and enzyme mechanistic communities.

The chemical basis for selection of the binuclear non-heme iron motif found in the active site of sMMO is as yet undefined in light of the observation that it is not the only enzymatic system capable of effecting the oxidation of alkanes. The cytochrome P_{450} family of enzymes and mononuclear, non-heme iron oxygenase enzymes are also capable of hydroxylating strong C−H bonds, and yet methanotrophs such as *M. capsulatus* (Bath), when grown

(78) Hsu, H. F.; Dong, Y.; Shu, L.; Young, V. G.; Que, L. *J. Am. Chem. Soc.* **1999**, *121*, 5230−5237.
(79) Price, J. C.; Barr, E. W.; Tirupati, B.; Bollinger, J. M.; Krebs, C. *Biochemistry* **2003**, *42*, 7497−7508.

under copper-deficient conditions, will express sMMO to supplement the copper-containing particulate methane monooxygenase (pMMO).[80] A search of the genome[81] of *M. capsulatus* reveals the presence of genes coding for cytochromes P_{450}, as well as mononuclear, non-heme iron enzymes, either of which might have been co-opted by evolutionary processes for the purpose of oxidizing methane. In laboratory studies, the heme-dependent cytochrome P450 BM-3 enzyme was subjected to directed evolutionary methods that resulted in the development of the previously absent ability to oxidize ethane (C−H bond strength 418 kJ mol^{-1}) to ethanol, demonstrating the potential for the heme scaffold to support thermodynamically challenging alkane oxidation chemistry.[82] Assuming that the presence of a binuclear iron center in sMMO is not arbitrary, one may question why nature chose to employ this motif. It is possible that the diiron(II) center of $sMMO_{red}$ has been tailored not only to facilitate the rapid, two-electron reduction of dioxygen to peroxide and formation of sMMO **P**, but for other unidentified reasons as well.[83]

The present study may provide a clue as to one additional use for the second iron center. In the absence of substrate, following the production of the active oxidant species, **3**, the ferryl-oxo collapses onto the neighboring Fe^{II} atom to form oxidatively and catalytically inert μ-oxo-[Fe^{III},Fe^{III}] **4**. A small, nonfunctionalized alkane like methane does not easily lend itself to an allosteric control mechanism by the enzyme or to a well-defined enzyme substrate binding site, so there is the possible danger that the powerful oxidant, kinetic **Q**, may form when the substrate is not immediately present at the iron site. In such an event, side chains in the active-site pocket may themselves be hydroxylated, thereby significantly altering the local hydrophobicity of the iron active-site environment in such a manner as to decrease the tendency of nonpolar alkanes to approach the iron core, resulting in diminished enzymatic activity. However, if **Q** is actually a diiron(IV) terminal mono oxo species, the presence of the second, nearby iron center in the binuclear core might provide a less-destructive decomposition pathway for the oxidant in the absence of methane. Such a pathway would generate a diferryl bridged-oxo species with a structure similar to the spectroscopically characterized **Q** (Scheme 4). Return to the resting diferric state could be accomplished by the introduction of exogenous electrons supplied by protein reductases in the presence of H^+.

It is certainly possible that the reactivity and catalytic behavior seen in studies of **1** are simply an alternative manifold of chemistry to that of sMMO, despite all of the similarities observed thus far. Such a possibility then raises an interesting set of questions regarding why nature has selected one pathway over another. If the chemistry of **1** and related complexes follows a mechanism distinct from the enzymatic processes, it will therefore be of interest to develop an understanding of why these differences occur. The model chemistry described in this investigation merely reflects transformations and processes that occur in a synthetic system. While such model information is useful as chemical constraints when thinking about possible enzymatic mechanisms, the relationships between reactivity models and enzyme active-site chemistry remain distant. Nonetheless, the detailed investigation of the chemistry of **1** and related complexes is important to further our understanding of binuclear iron-based oxygen-atom transfer catalysis. Detailed characterization of intermediates **2** and **3** are currently underway, and, in addition to revealing the nature of the species responsible for alkane oxidation, will help determine the biological relevance of this interesting chemistry to that which occurs in enzymatic systems.

Conclusion

Stopped-flow UV−vis spectroscopic studies have proven useful in the identification and assignment of intermediates that lie upon the catalytic and decay pathways of a non-heme diiron monooxygenase model compound. Reactions of OAD molecules with a synthetic [Fe^{II},Fe^{II}] compound, **1**, result in the formation of a high-valent Fe^{IV}═O intermediate, **2**, that undergoes reorganization to a catalytically competent intermediate, **3**. Reaction of **1** with one-electron oxidants provides support for the proposed rearrangement of the ligand framework that occurs following the initial oxygen-atom transfer step. Following reorganization of the high-valent iron-oxo complex, the complex undergoes intramolecular collapse to inert diferric μ-oxo **4**.

The electronic characteristics and reactivity of the proposed peroxide-bound intermediate species in sMMO, **P**, and the mechanism by which **P** converts to **Q**, are of fundamental interest. We showed previously that **1** induces heterolytic cleavage of the mechanistic probe peroxide MPPH and that it efficiently (>98%) catalyzes the conversion of cyclohexane to cyclohexanol (>300 turnovers).[39] Detailed stopped-flow kinetic mechanistic studies examining the reaction of peroxides with **1** and the subsequent generation of species **2**, **3**, and **4** (Scheme 1) are currently underway.

Acknowledgment. Financial support for this research was provided in part by the National Science Foundation (NSF 8238, JPC), the U.S. Department of Energy Office of Basic Energy Sciences (ER 14279, JPC), and the Department of Energy (DE-FG02-06ER15799, ERA). We thank the FMC corporation for their generous donation of 70% H_2O_2. *In memoriam* F.A.C., F.B.

Supporting Information Available: Eyring plots used to determine activation parameters, fits of the one-electron oxidation experimental data to kinetic models, ^{1}H NMR of **4**, and plots demonstrating reaction order and stoichiometry. This material is available free of charge via the Internet at http://pubs.acs.org.

IC7011217

(80) Lieberman, R. L.; Rosenzweig, A. C. *Crit. Rev. Biochem. Mol. Biol.* **2004**, *39*, 147−164.
(81) Ward, N.; Larsen, O.; Sakwa, J.; Bruseth, L.; Khouri, H.; Durkin, A. S.; Dimitrov, G.; Jiang, L. X.; Scanlan, D.; Kang, K. H. *et. al. PLoS Biol.* **2004**, *2* (10), 1616−1628.
(82) Meinhold, P.; Peters, M. W.; Chen, M. M. Y.; Takahashi, K.; Arnold, F. H. *ChemBioChem* **2005**, *6*, 1765−1768.
(83) Lipscomb, J. D.; Que, L. *J. Biol. Inorg. Chem.* **1998**, *3*, 331−336.